



# Tailored micro-optical freeform holograms for integrated complex beam shaping

SÖREN SCHMIDT,<sup>1,\*</sup> SIMON THIELE,<sup>2</sup> ANDREA TOULOUSE,<sup>2</sup> CHRISTOPH BÖSEL,<sup>4</sup> TOBIAS TIESS,<sup>3</sup> ALOIS HERKOMMER,<sup>2</sup> HERBERT GROSS,<sup>4</sup> AND HARALD GIESSEN<sup>5</sup>

<sup>1</sup>Corporate Research & Technology, Carl Zeiss AG, 07745 Jena, Germany

<sup>2</sup>Institute of Applied Optics (ITO) and Research Center SCoPE, University of Stuttgart, Germany

<sup>3</sup>Leibniz Institute of Photonic Technology, Albert-Einstein-Str. 9, 07745 Jena, Germany

<sup>4</sup>Institute of Applied Physics, Friedrich-Schiller-Universität Jena, 07743 Jena, Germany

<sup>5</sup>4th Physics Institute and Research Center SCoPE, University of Stuttgart, 70569 Stuttgart, Germany

\*Corresponding author: soeren.schmidt@zeiss.com

Received 14 April 2020; revised 5 July 2020; accepted 22 July 2020 (Doc. ID 395177); published 28 September 2020

Modern optical measurement technologies such as structured light microscopy or fringe-projection profilometry rely fundamentally on structured illumination of the specimen or probe. Miniaturizing the applied illumination concept enables the availability of these methodologies even in spatial domains that have remained inaccessible so far. Here we introduce a design methodology to realize complex illumination patterns with high diffraction efficiencies in a strongly miniaturized and functional integrated approach. This is achieved by combining the advantages of refractive freeform wavefront tailoring and diffractive beam shaping. This novel concept overcomes classical stray light issues known from conventional diffractive beam shaping and remains valid for micro-optical systems, i.e., beyond the geometric optical regime. Moreover, the design process is in particular optimized to reduce the aspect ratio of the obtained surface features. This strongly improves the manufacturability and as-built performance of the designed optical element, and the feasibility of the approach is demonstrated by the design and realization of monolithic beam shaping units on the tips of optical fibers via two-photon direct laser writing. This provides the means to realize complex illumination patterns in an integrated and mechanically flexible approach. © 2020 Optical Society of America under the terms of the OSA Open Access Publishing Agreement

<https://doi.org/10.1364/OPTICA.395177>

## 1. INTRODUCTION

The realization of specifically tailored intensity profiles of laser beams is of specific importance in a large variety of applications. For instance, in laser-based material processing, the quality of modified workpieces is critically linked to the intensity profile of the laser in the focal region [1]. Alternatively, for optical tweezers and atom traps, the light intensity distribution defines the trapping potential [2]. Moreover, structured illumination enables three-dimensional object reconstruction in fringe-projection profilometry [3] or facial recognition within modern mobile phone applications. Finally, tailored focal field distributions enable extended depth of field imaging [4,5] and allow for overcoming the classical resolution limit as defined by Abbe in structured light microscopy [6].

These field distributions are conventionally achieved by altering the phase of an initial laser beam by a specifically designed phase mask, e.g., a diffractive optical element (DOE) or a metasurface hologram (MSH). These components are usually placed in a Fourier-conjugated plane, i.e., the farfield or the focus of a Fourier imaging setup [7,8]. The DOEs are often purely diffractive with binary phase profiles and are therefore inherently very sensitive to

speckle effects, stray light, and the excitation of unwanted higher diffraction orders of the DOE [9]. Alternatively, MSHs can provide additional control over dispersive, polarization, and angular properties [10]. Nevertheless, the excitation of a zeroth diffraction order and unwanted stray light can similarly not be suppressed thoroughly [11,12] and the overall diffraction efficiency of MSHs was mentioned to be inferior compared to classical DOEs [13].

In contrast, refractive beam shaping concepts can overcome the mentioned limitations and realize target intensities with a high purity [14]. However, the underlying design algorithms rely on geometric optical concepts and neglect therefore any influence of diffraction [15]. As a consequence, the size of these systems needs to be rather macroscopic, resulting in severe drawbacks for the steady miniaturization of integrated optics. Overcoming these limitations is required to pave the way for novel applications [16–19].

In this paper, we introduce a design methodology that enables the realization of complex illumination patterns with high diffraction efficiencies and a simultaneous strong miniaturization of the beam shaping device. This is achieved by combining refractive freeform optical illumination concepts [14,15,20] with diffractive

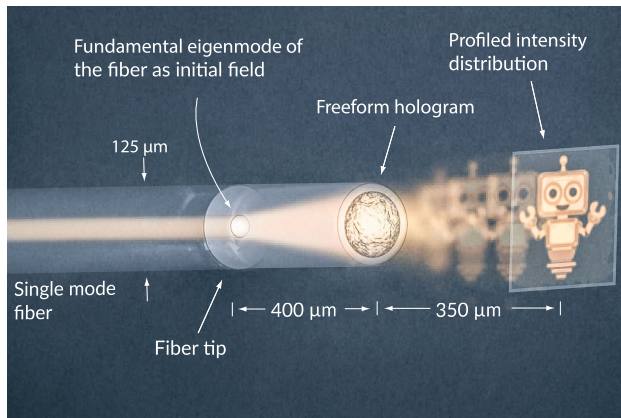


**Fig. 1.** Sketch of the integrated beam shaping setup: a freeform hologram surface is imprinted onto a homogeneous cylinder on the tip of an optical fiber manufactured by femtosecond two-photon direct laser writing. The fundamental eigenmode of the fiber is used as initial field, and inside the homogeneous cylinder the corresponding mode field diameter increases due to diffraction. The expanded mode field diameter at the cylinder tip reduces alignment sensitivities and increases the resolution in the realized target intensity. The freeform hologram profiles the phase of the incident beam and enables the redistribution of the field into the desired intensity.

beam shaping [21]. Roughly speaking, resulting surface profiles, which we term *freeform holograms*, are intended to be as refractive as possible and as diffractive as needed. On one hand, this allows suppression of diffractive stray light, i.e., one of the most severe challenges in diffractive beam shaping. On the other hand, the approach is not limited to the validity of a geometric optical regime, which would be the limitation of refractive beam shaping. In addition, our overall methodology might be interpreted as a novel formulation of the common phase retrieval problem [22] to result in specifically uniform and smooth phase profiles. Hence, our results may also be of particular interest for modern metrology [23,24] or microscopy techniques [25–27].

We demonstrate the feasibility of the proposed beam shaping approach by assessing two examples. On one hand, a focal beam shaping unit is established, which realizes a micrometer scaled target intensity in close vicinity to the freeform hologram (see Fig. 1). As a second example, a farfield projection unit is realized, which projects the target intensity to infinity. In both cases, the freeform hologram is monolithically integrated onto the tip of a single-mode optical fiber by femtosecond two-photon direct laser writing (see Fig. 1). This additive manufacturing technique enables the realization of highly accurate, complex three-dimensional micro-optical components [19,28–41] even on optical fiber tips [42–48].

During fabrication an optimized alignment of the freeform hologram and the fiber tip can be realized by observation via the printing microscope objective. Hence, after the manufacturing process, any additional alignment sensitivities are avoided, as the fabricated parts are positioned strictly to the fiber tip. In addition, the mechanical flexibility of the fiber is maintained, which enables high versatility of the device. This will open up novel experimental opportunities where structured illumination can be used in previously inaccessible domains. This could be of particular interest in microscopy, endoscopy, micro-surgery, optical trapping,

and lab-on-chip devices. Additionally, the high diffraction efficiencies improve the signal-to-noise ratio in these applications substantially.

To assess the manufactured beam shaping unit, topographic measurements of the fabricated surface profile and measurements of the realized intensity distribution are used. This allows evaluation of both the accuracy of manufacturing and the functionality of the device.

## 2. DESIGN

Shaping an initial beam into a target field distribution, in general, is realized by two different approaches, namely, refractive and diffractive beam shaping. The prior considers the redirection of an initial ray density distribution into a desired pattern in a distant plane, which permits to realize the target intensity distribution. This ray redistribution is described by a specific mapping function, which defines the reallocation of individual rays between initial and target planes. This can be realized by a specific freeform surface, which refracts the initial rays according to the mapping function [14]. Then, individual rays in the initial plane become either focused or defocused, which results in an energy concentration or spreading in a final target plane and permits to realize the final target intensity. Overall, this approach results in a smooth freeform surface without discontinuities, which prevents stray light and speckle effects [49]. Modern design methods [15] consider an optimal mapping approach that enables minimal deflection angles of the individual rays. Roughly speaking, this corresponds to a smallest possible numerical aperture (NA) of the beam shaping unit, which ensures a maximum depth of field in the realized intensity distribution. Moreover, the minimal deflection angles correspond to surface profiles with strongly reduced gradients. Hence, this suppresses surface features with high aspect ratios, which improves the manufacturability of the designed surface profiles, e.g., by diamond turning processes. Remaining surface deviations due to manufacturing imperfections will cause errors in the ray redistribution between initial and target planes, which may be interpreted as a disturbance of the ray-mapping function. Then manufacturing inaccuracies cause slight uniformity errors in a realized target intensity.

As a major limitation, the overall optical design process relies entirely on a geometric optical approach, which neglects any influences caused by the wave-optical nature of light. This is of special importance for the intended micro-optical scale in our case, where characteristic feature sizes become comparable to the considered wavelengths. (Additional information about refractive beam shaping principles is provided in Supplement 1.)

Alternatively, classical diffractive beam shaping considers the tailored superposition of individual plane waves at a given wavelength  $\lambda$ . Then, in contrast to refractive beam shaping, also coherent interference effects in between the individual waves are used to realize the target intensity. This utilization of interference effects makes the entire beam shaping process sensitive to local phase differences between the interfering waves, which is not the case for refractive beam shaping. This aspect increases accuracy requirements for manufacturing of the DOEs.

Within diffractive beam shaping, the phase of an initial monochromatic beam is altered by a specifically designed computer generated hologram (CGH). Then, the target intensity is typically realized in a Fourier conjugated plane, i.e., the farfield or the focus of a Fourier imaging setup. These CGHs are designed

mostly by modified formulations [21,22,50,51] of the original Gerchberg–Saxton algorithm, i.e., the iterative Fourier transform algorithm (IFTA) [52,53]. Manufacturing imperfections, e.g., edge rounding in direct laser writing [54] or a coarse layering of the height profile by conventional mask-based lithography, can result in the excitation of undesired diffraction orders, stray light, or speckle effects, which requires special care during the design of these DOEs [49,50,55–61].

It is the aim of our design approach to introduce a methodology that does not neglect wave-optical influences and keeps a designed surface as close as possible to a refractive solution. Roughly speaking, zeroth order stray light and speckle effects will be suppressed by the refractive part, while a minimum of diffractive structures is maintained to also realize fine details of the target intensity distribution, which otherwise appear to be blurred.

To reduce high spatial frequency features in resulting surface profiles, it was already proposed to use a refractive beam shaping solution within conventional IFTA routines as an initial phase guess [49,62]. Moreover, it was suggested to gradually change the unperturbed beam profile in the target plane to a desired field distribution within the design process to ensure a smooth convergence of the IFTA routine [63,64]. While these procedures improve the original IFTA algorithm, they nevertheless cannot directly restrict the diffractive surface part, i.e., the deviation of the surface from the refractive solution. As a consequence, the diffractive surface part may vary arbitrarily within the design process, and the manufacturability of designed surface profiles remains challenging.

Alternatively, we will introduce a design algorithm that directly assesses and restricts the deviation of a final surface profile from the refractive solution. To this end, a refractive beam shaping solution, which is described by the unwrapped geometrical phase  $\Delta\varphi_{\text{Refr.}}(x, y)$ , will gradually be modified by an adapted IFTA-type algorithm. The IFTA algorithm naturally modifies the absolute phase of the beam, which is the superposition of the induced phase by the refractive freeform element  $\Delta\varphi_{\text{Refr.}}(x, y)$  and the unwrapped initial phase  $\phi_0(x, y)$  of the incoming beam. This superposition can be interpreted as a refractive beam shaping solution for collimated incident light  $\Delta\varphi_{\text{Refr.}}^{\text{Coll.}}(x, y) = \Delta\varphi_{\text{Refr.}}(x, y) + \phi_0(x, y)$ .

Then, within individual optimization cycles  $j$ , the current unwrapped phase profile  $\Delta\varphi^j(x, y)$  is not allowed to vary arbitrarily, and the diffractive phase part  $\Delta\varphi_{\text{Diff.}}^j(x, y) = \Delta\varphi^j(x, y) - \Delta\varphi_{\text{Refr.}}^{\text{Coll.}}(x, y)$  is restricted in every optimization cycle. In particular, the emergence of any grating-type structures in the diffractive phase profile should be suppressed as well as possible. This is achieved by low-pass filtering the diffractive phase profile  $\Delta\varphi_{\text{Diff.}}^j(x, y)$  in every optimization cycle by a convolution with a Gaussian function, and the phase in the next iteration  $j + 1$  reads as

$$\Delta\varphi^{j+1}(x, y) = \Delta\varphi_{\text{Refr.}}^{\text{Coll.}}(x, y) + \Delta\varphi_{\text{Diff.}}^j(x, y) \otimes e^{-\left(\frac{x^2+y^2}{2\sigma^2}\right)}.$$

During the optimization, the width  $\sigma$  of this blurring filter is gradually reduced. Hence, any higher spatial frequency content in the diffractive phase part can only gradually rise with the reduction of the blurring kernel. After an optimization has terminated, the unwrapped initial phase  $\phi_0(x, y)$  is subtracted from the optimized solution  $\Delta\varphi^{\text{end}}(x, y)$ , and the phase of the freeform hologram reads as  $\Delta\varphi(x, y) = \Delta\varphi^{\text{end}}(x, y) - \phi_0(x, y)$ .

(Detailed information on the optimization algorithm is provided in Supplement 1.).

One may interpret a freeform hologram as a beam shaping surface that is intended to be as smooth as possible, i.e., characterized by a reduced spatial frequency content of the surface profile. This can improve the manufacturability and thus the as-built performance of designed freeform holograms. In particular, femtosecond two-photon 3D-direct laser writing is considered for fabrication, which enables the realization of three-dimensional surface profiles without a coarse layering of the structure at the price of reduced lateral resolutions compared to mask-based lithographic concepts. Then, a manufacturing imperfection may be understood as a low-pass filtering of the surface profile according to the voxel size of the focused beam used in direct laser writing [54]. This effect of a manufacturing imperfection affects a realized surface profile similar to the filtering process of the overall design procedure. Hence, a rounding of the continuous and smooth surface relief caused by manufacturing imperfections is less problematic compared to wrapped surface profiles of conventional DOEs, where edge roundings are critical [54].

Overall, the optical design of freeform holograms relies on the restriction of the diffractive phase part. This, of course, requires explicit knowledge of a refractive beam shaping solution, which usually is not easily available, as the underlying algorithms are complex [15,20]. Alternatively, we would like to first demonstrate the robustness of our proposed design procedure, to result in manufacturable freeform holograms even without explicit knowledge of a refractive solution. To this end, a constant phase profile was chosen initially within the design process, and the considered beam shaping scenario is depicted in Fig. 1. Then, the propagated eigenmode of the fiber at the position of the freeform hologram is used within the freeform hologram design, and subsequent results calculated with MATLAB are shown in Fig. 2. More generally, we suggest to use a wavefront of the form  $\Delta\varphi_{\text{Refr.}}(x, y) = ax + by + cx^2 + dxy + ey^2$ , which corresponds to a second-order Taylor approximation of the refractive beam shaping phase and allows to adapt the target intensity distribution by an elliptical profile. The coefficients  $a - e$  may be retrieved by a numerical optimization routine to yield a best approximation of the target intensity by an elliptical profile. (Additional information about a connection between the parameters  $a - e$  and underlying system properties of the beam shaping setup is provided within Supplement 1.).

While the quality of a realized target intensity is influenced mostly by the design methodology, an overall achievable resolution in the target intensity is linked to an initial mode field diameter (MFD), which illuminates the freeform hologram. It determines the smallest feature sizes that can be realized in an otherwise ideal system. This influence is explained by the Rayleigh criterion, which connects the MFD to an angular resolution  $\Delta\theta \approx 1.22 \frac{\lambda}{\text{MFD}}$ . In conventional diffractive beam shaping, i.e., CGH and target planes are Fourier conjugated, the smallest feature details in the target intensity are described directly by this angular resolution  $\Delta\theta$ . Hence, a large MFD can improve the quality of a realized target field distribution. Alternatively, for a finite distance  $z_{\text{Target}}$  between the freeform hologram and the target field distribution, the angular resolution might be converted into spatial domain  $\Delta x = 1.22 \frac{\lambda}{\text{MFD}} z_{\text{Target}}$  by identifying  $\Delta\theta \approx \frac{\Delta x}{z_{\text{Target}}}$ . In addition, an increased MFD lowers alignment sensitivities of the freeform hologram with respect to the fiber core as well [45].

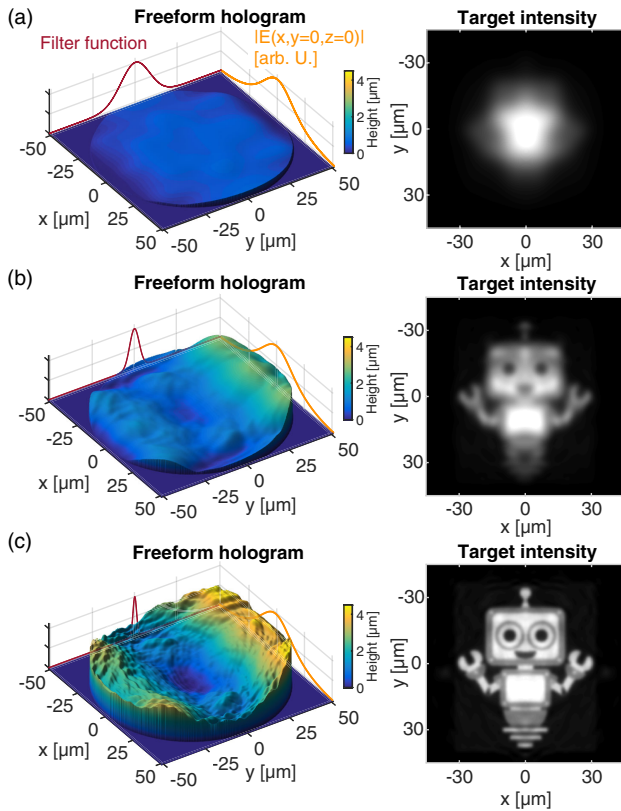


**Fig. 2.** Intermediate results of the freeform hologram design process, where a constant phase profile was chosen initially within the design process. Feature sizes in the surface sag are gradually increasing during the design procedure. This is realized by a Gaussian filtering of the surface sag, where the corresponding width is adapted during iterations. This allows a smooth convergence of the design algorithm and avoids the appearance of large gradients in the surface sag. (a)–(c) Design results of individual iteration steps. Respectively, the surface sag is shown on the left and the corresponding intensity in the target plane  $|E(x, y, z_{\text{Target}})|^2$  on the right. Note: at the boundaries of the plot, a profile of the field amplitude  $|E(x, y, z = 0)|$  and the filter function have been added to provide additional information connected to the design of the surface sag.

The MFD is increased in our approach by allowing the fundamental eigenmode of the fiber to propagate in a homogeneous medium prior to being modified by the freeform hologram (see also Fig. 1). This way the beam expands due to diffraction, and the divergence is characterized by the NA of the fiber.

The thin-element approximation (TEA) is used to convert the retrieved phase change  $\Delta\varphi(x, y)$  into a surface profile  $z(x, y)$ . The topography of the freeform hologram is then described as  $z(x, y) = \frac{\Delta\varphi(x, y)}{\Delta n k_0}$ , where  $\Delta n$  describes the index contrast, and  $k_0 = \frac{2\pi}{\lambda}$  is the wavenumber of light with a wavelength  $\lambda$  in vacuum. In a strict sense, the TEA remains valid only for the description of thin structures in the range of a few wavelengths [65]. To assess the validity of the chosen TEA, additional simulations of the designed freeform holograms are considered with the wave propagation method [66]. This algorithm enables an accurate virtual prototyping of micro-optical elements [65,67,68], and a potential final design is analyzed prior to a manufacturing step and accepted only if it provides satisfying results.

### 3. REALIZATION

The designed freeform holograms were fabricated via femtosecond direct laser writing, performed using a Nanoscribe Professional GT setup in dip-in configuration. As a photopolymer, IP-DIP was chosen, which is optimized for highest resolution and shape accuracy. The writing objective features a NA of  $\text{NA} = 1.4$ , which leads to a lateral voxel size of approximately 200 nm and a typical elongation of 500 nm. The optimum process window was determined by a systematic investigation of the parameter space using the final freeform surface. Printed on a glass substrate (BK7,  $t = 170 \mu\text{m}$ ), the results were investigated in terms of shape accuracy as well as optical performance after varying process parameters, e.g., laser power and slicing distance. Further details about the manufacturing process can be found in [44].

In a first example, the focal beam shaping unit, which was introduced and discussed in Section 2, will be realized. To this end, the fundamental eigenmode of a Thorlabs SM-630HP fiber, specified with a NA of  $\text{NA} = 0.12$  and a core diameter of  $D_{\text{Core}} = 3.5 \mu\text{m}$ , is considered. As a light source, a fiber-coupled LED (Thorlabs LED M625F2) at a wavelength of  $\lambda \approx 0.63 \mu\text{m}$  is used. Then the eigenmode expands inside the homogeneous cylindrical part, and its length is chosen to result in a MFD of about  $50 \mu\text{m}$ . Hence, the MFD is chosen smaller than the fiber diameter, which takes into account that within the MFD of a Gaussian beam, only 86% of the total energy is encircled. By choosing the MFD considerably larger, diffraction effects originating from the surrounding edges of the beam shaping unit might disturb a realized target intensity. In the considered scenario, the spherical phase of the propagated fundamental eigenmode is neglected. As a consequence, the target field distribution becomes slightly magnified, which simplifies the microscopic assessment of the profiled intensity distribution. Otherwise, also an additional negative spherical phase could be added to the designed phase profile to compensate for the phase of the incident beam.

To evaluate the realized beam shaping unit, the surface topography of the freeform hologram is evaluated by a confocal surface measurement (Nanofocus  $\mu$  surf expert) in a first step. This allows us to directly compare designed and measured surface profiles and to evaluate the manufacturing quality (see Fig. 3). To quantitatively determine the quality of the realized freeform hologram, we calculate the total root-mean-square difference (RMS) between the measured and designed surface

$$\text{RMS} = \sqrt{\frac{\iint_D |z_{\text{Meas}}(x, y) - z_{\text{Design}}(x, y)|^2 dx dy}{\iint_D dx dy}},$$

where  $D$  is the diameter of the freeform hologram. A RMS error of about 60 nm was realized. This corresponds to a minor wavefront error  $\Delta\varphi_{\text{RMS}} = k_0 \Delta n \text{RMS}$  of approximately  $\frac{1}{20}$  of a full phase cycle for the considered wavelength of  $\lambda = 0.63 \mu\text{m}$ , which is considered to be diffraction limited within a conventional optical system design.

To predict the performance of the beam shaping unit including the measured surface deviations, we perform simulations in MATLAB with the wave propagation method. Additionally to the original design, here also the spectral characteristics of the illumination are considered. To this end, individual simulations at varying wavelengths weighted by the spectrum are added incoherently. In particular, we considered the spectral bandwidth  $\Delta\lambda \approx 15 \text{ nm}$  of the fiber coupled LED (Thorlabs M625F2) within the numerical simulations. A comparison of the simulations for the ideal freeform hologram and one considering the

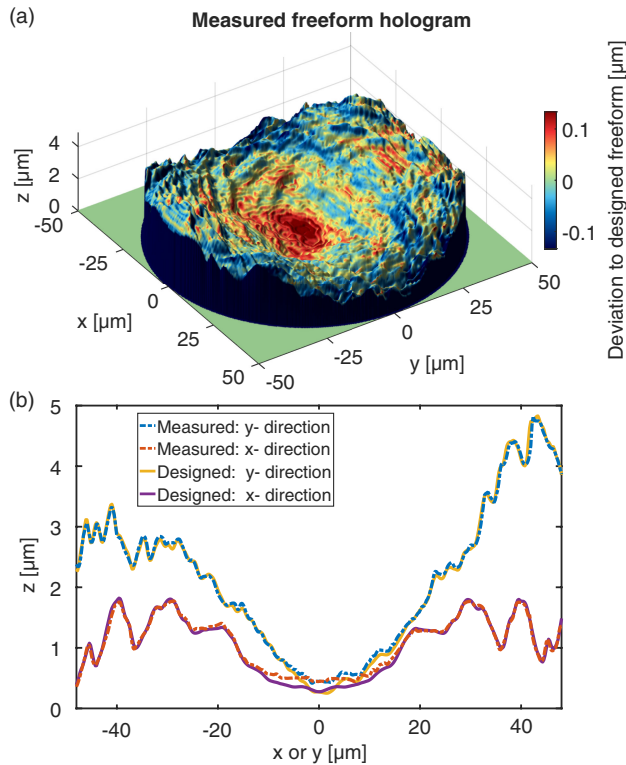


**Fig. 3.** (a) Measured surface sag of the freeform hologram ( $z$  axis) and superimposed deviation (color bar) from the design. (b) Comparison between the measured and designed freeform holograms along the coordinate axes  $z(x=0, y)$ ,  $z(x, y=0)$ .

measured topography of a realized freeform hologram is shown in Figs. 4(a) and 4(b). Even the small dots, e.g., at the wrist of the robot image, are resolved, which indicates the high accuracy of the manufactured freeform. In a final step, the target intensity was measured using a microscope setup consisting of a  $50\times$  /NA 0.55 Mitutoyo microscope lens, a tube system, and a camera (IDS UI-3180CP-C-HQ). The corresponding result is shown in Fig. 4(c). A linear gradient of intensity is realized in the measured image. This can be explained by a decentering of the Gaussian intensity distribution at the position of the freeform hologram with respect to the center of the surface (see Supplement 1 for supporting content). This might be caused by a non-ideal cleave of the fiber tip, a tilt of the imprinted cylinder relative to the fiber, or a decentered alignment. This changes the optical axis of the beam and causes a decentering on the freeform hologram. This issue can be resolved by aligning the imprinting process with respect to the center of gravity of the initial field after the realization of the cylinder. Hence, this slight deviation between simulation and experiment originates solely from the fabrication procedure.

It is evident that neither strong speckle artifacts nor a notable excitation of a zeroth or higher diffraction order is apparent within the measurement. However, one can realize some imperfections in the uniformity of the intensity distribution. This is caused by surface imperfections of the manufacturing process and may be explained based on the principles of refractive beam shaping. In particular, shape deviations cause slight errors in the ray-mapping function, which describes the ray redistribution between initial and target planes and results in the mentioned non-uniformity. To also quantitatively judge the accuracy of the realized intensity distribution, the maximum value of the normalized 2D cross-correlation

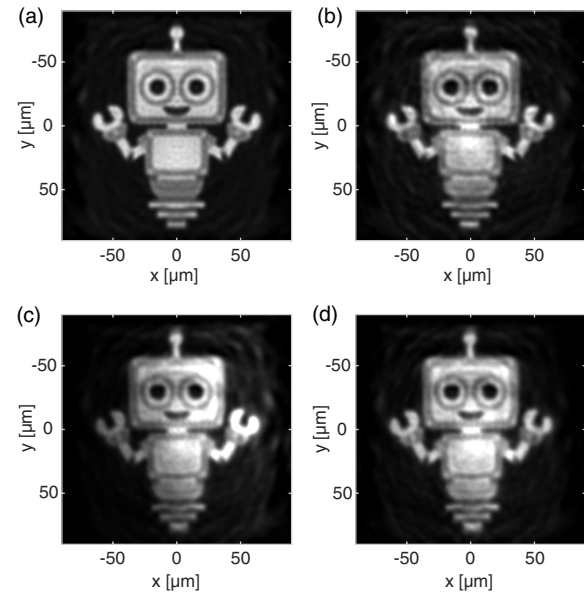


**Fig. 4.** (a), (b) Simulation of the ideal freeform hologram in comparison to a simulation where the measured topography of a manufactured freeform hologram is assessed. The simulations were performed with the wave propagation method, and individual results for varying wavelengths were added incoherently to account for the spectral bandwidth  $\Delta\lambda \approx 15$  nm of the illumination source (Thorlabs LED M625F2). (c) Measurement of the profiled intensity distribution in the target plane of the realized beam shaping unit. (d) To enhance the visibility of the measured intensity, the recorded image was modified by a graduated intensity filter, which corresponds to the multiplication by a linear function. (a)–(d) Each image is normalized by its total integrated power, and all images share the same color map.

between the measured and simulated images is evaluated numerically [69]. Respectively, values of 0.90 and 0.91 are found relying on the simulations of the ideal and the measured topography of the freeform. To estimate the accuracy of the realized focal field distribution without decentration error, we consider a digital adaptation of the measured intensity. Hence, a gradual intensity filter is applied to the measured focal field distribution. This corresponds to the multiplication of the measured intensity with a properly aligned linear function. This enhances the visibility of the smallest realized feature details in the focal field distribution and improves the assessment. These results are shown in Fig. 4(d). Again, the individual dots of the robot image are resolved, which underlines the accuracy of the approach. The measured intensity pattern appears visually even with an improved accuracy compared to the simulated results in Fig. 4(b). This might be explained by errors of the topography measurements, which lead to an increased deviation between measured and designed surfaces, which, of course, influences the simulations. For the adapted measurement, the correlation coefficient is evaluated again. In this case, values of 0.96 and 0.97 are found relying on the simulations of the ideal and the measured topography of the freeform, respectively.

Until now, a beam shaping unit was assessed that realizes a micrometer scaled target intensity in close vicinity of approximately  $400\ \mu\text{m}$  behind the freeform hologram. This could be of special interest in microscopy and for optical trapping. In particular, the close distance in between the freeform hologram surface and the realized target intensity is advantageous. Then, in contrast to classical farfield approaches, there is only a short

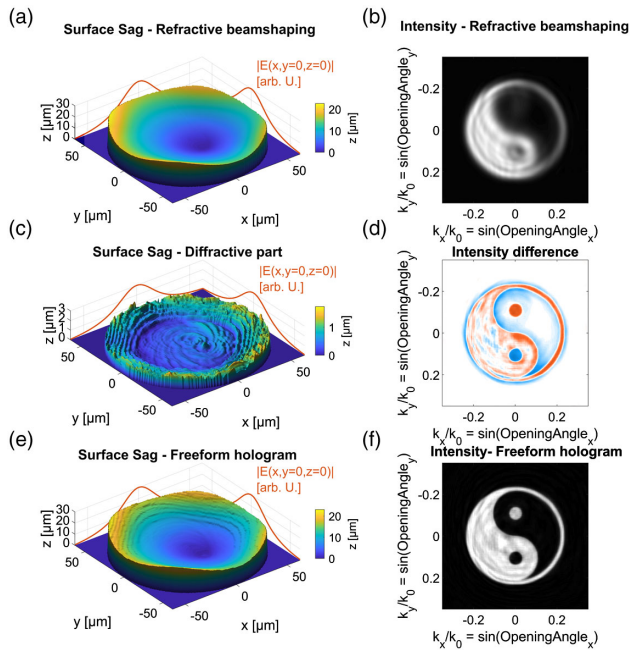


**Fig. 5.** (a), (c), (e) Surface sags of the refractive beam shaping solution, the pure diffractive part, and the freeform hologram as superposition of the refractive and diffractive part to redistribute the initial Gaussian eigenmode in the farfield into a Yin Yang symbol [please note the different height scales in (c)]. (b), (f) Simulations of the farfield intensity distributions of the refractive and freeform hologram solutions. There, the farfield intensity is simulated as  $|\tilde{E}(k_x, k_y)|^2 = |\iint E_0(x, y) e^{-i(k_x x + k_y y)} dx dy|^2$ , where  $E_0(x, y)$  is the complex field directly behind the freeform hologram. (d) Intensity difference between refractive and freeform hologram solutions. The red color highlights regions of missing intensity in the refractive beam shaping solution, whereas the blue color highlights overexposed areas in the refractive solution. Note: at the boundaries of the plot, a profile of the field amplitude  $|E(x, y, z = 0)|$  has been added to provide additional information connected to the design of the surface sag.

propagation distance to the actual target position, and structured illumination can be used deep inside turbid media, where scattering processes inside the tissue are one of the most severe challenges [18,70].

In a final step, a second beam shaping unit was designed and realized, which projects the target intensity to infinity. This highlights the opportunities of the methodology for classical projection purposes, e.g., for fringe projection. In this example, the freeform hologram is designed to realize a Yin Yang symbol in the farfield. Within the optimization process, a refractive beam shaping solution was considered [15], and subsequent results are shown in Fig. 5. In particular, Figs. 5(a) and 5(b) show the refractive beam shaping surface and the related intensity in the farfield. Clearly, the actual target intensity is not accurately realized by the refractive beam shaping surface and appears to be blurred. This is caused by diffractive influences, which are not considered within the geometrical refractive beam shaping models. Moreover, Figs. 5(e) and 5(f) show the surface profile of the freeform hologram and the connected farfield intensity. The improvement in the realized target intensity is clearly evident and caused directly by the diffractive phase contribution in the freeform hologram. To analyze this aspect in a little more detail, Figs. 5(c) and 5(d) depict the diffractive surface profile and its impact on the realized target intensity. To be more precise, Fig. 5(d) shows the intensity difference between

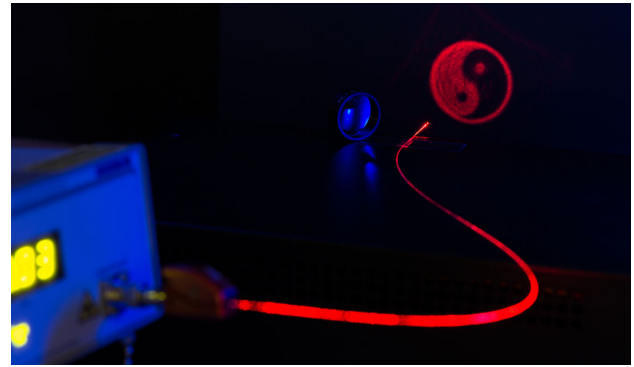


**Fig. 6.** Photograph of the realized farfield intensity distribution and the imprinted optical fiber. A lens with an approximate diameter of 25 mm is added to the photograph to serve as dimensional reference.

the refractive and freeform hologram solutions. In particular, a blue color highlights overexposed intensity regions in the refractive solution, and vice versa, a red color highlights underexposed areas. Hence, one might interpret the diffractive phase part in the freeform hologram as a means to redistribute under- and overexposed intensities in the refractive solution to yield the ideal target intensity.

By taking a closer look at Fig. 5(c), one realizes a rather flat plateau within the diffractive phase part with only a weak diffractive structure in the inner regions of the freeform hologram. For larger distances from the optical axis, the diffractive part in the freeform hologram is becoming slightly stronger. However, these parts are lying outside the actual MFD of the initial beam, i.e., at the tails of weak intensity of the initial beam. Hence, these parts in the freeform hologram are of only subordinate importance for the beam shaping process. The reduced and overall small proportion of the diffractive part in the freeform hologram underlines the ability of the proposed design methodology to suppress diffractive structures in the resulting surface as well as possible.

In the next and final step, the freeform hologram is realized and evaluated experimentally. In this case, the homogeneous cylinder was realized by a spliced piece of a silica no-core fiber (Thorlabs FG125LA) with a length of  $l = 470 \mu\text{m}$  and a diameter of  $D = 125 \mu\text{m}$ . Prior to imprinting the freeform hologram, the eigenmodal profile was experimentally assessed, and the results were incorporated within the design process. In particular, the NA of the fiber was experimentally assessed, which lowers influences caused by fabrication tolerances of the used SM600 fiber from Thorlabs. As an illumination source, a fiber coupled laser (Thorlabs S1FC635) operating at a wavelength of  $\lambda = 635 \text{ nm}$  was used. The resulting farfield intensity profile is shown in Fig. 6.

In this example, one can realize some speckle influences in the measurement by comparing the simulated farfield distribution with the experimental assessment. This effect is caused strictly by subjective speckles originating from the rough surface being illuminated by a coherent laser illumination. Apart from these influences, the comparison between simulation and measurement is in good agreement.

#### 4. CONCLUSION

In summary, we introduced a design methodology to realize complex illumination patterns for highly miniaturized applications. To

this end, the advantages of refractive freeform wavefront tailoring approaches were combined with diffractive beam shaping. As a result, designed surface profiles are characterized by a smooth three-dimensional surface profile without strong gradients and thus low aspect ratios. On one hand, this suppresses diffractive stray light thoroughly, i.e., one of the most severe challenges in diffractive beam shaping. On the other hand, this lowers the technological requirements towards the manufacturing process, i.e., femtosecond two-photon direct laser writing, significantly. There, the resolution of the smallest feature sizes in a realized surface profile sensitively depends upon a considered writing objective, a used photoresist, and additional process parameters. Hence, lowering these requirements improves the as-built quality and thereby the functionality of freeform holograms. Thus, the adapted design strategy enables the realization of complex illumination patterns in a highly integrated approach.

The feasibility of the proposed approach has been demonstrated by monolithically integrating designed beam shaping units onto tips of single-mode optical fibers. A topographic measurement of a realized freeform hologram shows an excellent agreement with the designed one, which underlines the as-built quality of the realized surface profiles. In the next step, the realized target intensities have been assessed experimentally. On one hand, a focal beam shaping unit, which realizes a micrometer scaled target intensity, has been assessed by a microscopic measurement. On the other hand, a farfield beam shaping unit has been investigated. In both cases, the exceptional functionality of the beam shaping units were confirmed and thus the unique ability to realize complex illumination patterns in a highly integrated approach. In the future, our approach might be utilized for complex optical tweezers, within integrated lidar or augmented and virtual reality (AR/VR) projection systems, for structured light microscopy, or as enabling technology to merge fringe projection profilometry with endoscopy.

**Funding.** Bundesministerium für Bildung und Forschung (KoSimO, Post-Grant-Fund, PRINTFUNCTION, PRINTOPTICS); European Research Council (Advanced Grant (ComplexPlas), POC Grant (3DPrintedOptics)); Deutsche Forschungs Gemeinschaft (SPP1839); Baden-Württemberg Stiftung (OPTERIAL, Spitzenforschung II).

**Acknowledgment.** We would like to thank Robert Röder from the Institute of Solid State Physics in Jena for stimulating discussions, Moritz Floess from 4th Physics Institute in Stuttgart for taking the photograph in Fig. 6, Teresa Pfau and Claudia Imiolczyk from 4th Physics Institute in Stuttgart for splicing the fibers and experimental support. Photo credits: the robot image was modified from the original image under: <https://commons.wikimedia.org/wiki/File:Robot-clip-art-book-covers-feJCV3-clipart.png>.

**Disclosures.** The authors declare no conflicts of interest.

See Supplement 1 for supporting content.

## REFERENCES

- P. S. Salter and M. J. Booth, "Adaptive optics in laser processing," *Light Sci. Appl.* **8**, 110 (2019).
- A. Jesacher, C. Maurer, A. Schwaighofer, S. Bernet, and M. Ritsch-Marte, "Full phase and amplitude control of holographic optical tweezers with high efficiency," *Opt. Express* **16**, 4479–4486 (2008).
- C. Zuo, S. Feng, L. Huang, T. Tao, W. Yin, and Q. Chen, "Phase shifting algorithms for fringe projection profilometry: a review," *Opt. Laser Eng.* **109**, 23–59 (2018).
- P. Zammit, A. R. Harvey, and G. Carles, "Extended depth-of-field imaging and ranging in a snapshot," *Optica* **1**, 209–216 (2014).
- S. Banerji, M. Meem, A. Majumder, B. Sensale-Rodriguez, and R. Menon, "Extreme-depth-of-focus imaging with a flat lens," *Optica* **7**, 214–217 (2020).
- M. G. Gustafsson, "Surpassing the lateral resolution limit by a factor of two using structured illumination microscopy," *J. Microsc.* **198**, 82–87 (2000).
- A. Forbes, A. Dudley, and M. McLaren, "Creation and detection of optical modes with spatial light modulators," *Adv. Opt. Photon.* **8**, 200–227 (2016).
- A. Forbes, "Structured light from lasers," *Laser Photon. Rev.* **13**, 1900140 (2019).
- G. Swanson and L. Laboratory, "Binary optics technology: the theory and design of multi-level diffractive optical elements," Technical Report (Lincoln Laboratory/Massachusetts Institute of Technology, 1989).
- S. M. Kamali, E. Arbabi, A. Arbabi, and A. Faraon, "A review of dielectric optical metasurfaces for wavefront control," *Nanophotonics* **7**, 1041–1068 (2018).
- G. Zheng, H. Mühlenbernd, M. Kenney, G. Li, T. Zentgraf, and S. Zhang, "Metasurface holograms reaching 80% efficiency," *Nat. Nanotechnol.* **10**, 308–312 (2015).
- G. Yoon, D. Lee, K. T. Nam, and J. Rho, "Pragmatic metasurface hologram at visible wavelength: the balance between diffraction efficiency and fabrication compatibility," *ACS Photon.* **5**, 1643–1647 (2017).
- S. Banerji, M. Meem, A. Majumder, F. G. Vasquez, B. Sensale-Rodriguez, and R. Menon, "Imaging with flat optics: metalenses or diffractive lenses?" *Optica* **6**, 805–810 (2019).
- H. Ries and J. Muschaweck, "Tailored freeform optical surfaces," *J. Opt. Soc. Am. A* **19**, 590–595 (2002).
- C. Bösel and H. Gross, "Ray mapping approach for the efficient design of continuous freeform surfaces," *Opt. Express* **24**, 14271–14282 (2016).
- C. Liberale, P. Minzioni, F. Bragheri, F. D. Angelis, E. D. Fabrizio, and I. Cristiani, "Miniaturized all-fibre probe for three-dimensional optical trapping and manipulation," *Nat. Photonics* **1**, 723–727 (2007).
- S. Juodkazis, "Manufacturing: 3D printed micro-optics," *Nat. Photonics* **10**, 499–501 (2016).
- I. T. Leite, S. Turtaev, X. Jiang, M. Šiler, A. Cuschieri, P. St. J. Russell, and T. Čizmar, "Three-dimensional holographic optical manipulation through a high-numerical-aperture soft-glass multimode fibre," *Nat. Photonics* **12**, 33–39 (2017).
- P.-I. Dietrich, M. Blaicher, I. Reuter, M. Billah, T. Hoose, A. Hofmann, C. Caer, R. Dangel, B. Offrein, U. Troppenz, M. Moehle, W. Freude, and C. Koos, "In situ 3D nanoprinting of free-form coupling elements for hybrid photonic integration," *Nat. Photonics* **12**, 241–247 (2018).
- C. Bösel and H. Gross, "Single freeform surface design for prescribed input wavefront and target irradiance," *J. Opt. Soc. Am. A* **34**, 1490–1499 (2017).
- O. Ripoll, V. Kettunen, and H. P. Herzig, "Review of iterative Fourier-transform algorithms for beam shaping applications," *Opt. Eng.* **43**, 2549 (2004).
- J. R. Fienup, "Phase retrieval algorithms: a comparison," *Appl. Opt.* **21**, 2758–2769 (1982).
- B. M. Hanser, M. G. L. Gustafsson, D. A. Agard, and J. W. Sedat, "Phase retrieval for high-numerical-aperture optical systems," *Opt. Lett.* **28**, 801–803 (2003).
- S. Merx, J. Stock, F. R. Widiarsari, and H. Gross, "Beam characterization by phase retrieval solving the transport-of-intensity-equation," *Opt. Express* **28**, 20898–20907 (2020).
- G. Zheng, R. Horstmeyer, and C. Yang, "Wide-field, high-resolution Fourier ptychographic microscopy," *Nat. Photonics* **7**, 739–745 (2013).
- L.-H. Yeh, J. Dong, J. Zhong, L. Tian, M. Chen, G. Tang, M. Soltanolkotabi, and L. Waller, "Experimental robustness of Fourier ptychography phase retrieval algorithms," *Opt. Express* **23**, 33214–33240 (2015).

27. T. Aidukas, R. Eckert, A. R. Harvey, L. Waller, and P. C. Konda, "Low-cost, sub-micron resolution, wide-field computational microscopy using open-source hardware," *Sci. Rep.* **9**, 7457 (2019).
28. Q.-D. Chen, D. Wu, L.-G. Niu, J. Wang, X.-F. Lin, H. Xia, and H.-B. Sun, "Phase lenses and mirrors created by laser micromanufacturing via two-photon photopolymerization," *Appl. Phys. Lett.* **91**, 171105 (2007).
29. G. von Freymann, A. Ledermann, M. Thiel, I. Staude, S. Essig, K. Busch, and M. Wegener, "Three-dimensional nanostructures for photonics," *Adv. Funct. Mater.* **20**, 1038–1052 (2010).
30. M. F. Schumann, S. Wiesendanger, J. C. Goldschmidt, B. Bläsi, K. Bittkau, U. W. Paetzold, A. Sprafke, R. B. Wehrspohn, C. Rockstuhl, and M. Wegener, "Cloaked contact grids on solar cells by coordinate transformations: designs and prototypes," *Optica* **2**, 850–853 (2015).
31. A. Žukauskas, M. Malinauskas, and E. Brasselet, "Monolithic generators of pseudo-nondiffracting optical vortex beams at the microscale," *Appl. Phys. Lett.* **103**, 181122 (2013).
32. M. Malinauskas, A. Žukauskas, S. Hasegawa, Y. Hayasaki, V. Mizeikis, R. Buividas, and S. Juodkzasis, "Ultrafast laser processing of materials: from science to industry," *Light Sci Appl.* **5**, e16133 (2016).
33. S. Lightman, G. Hurvitz, R. Gvishi, and A. Arie, "Tailoring lens functionality by 3D laser printing," *Appl. Opt.* **56**, 9038–9043 (2017).
34. S. Lightman, G. Hurvitz, R. Gvishi, and A. Arie, "Miniature wide-spectrum mode sorter for vortex beams produced by 3D laser printing," *Optica* **4**, 605–610 (2017).
35. P.-I. Dietrich, R. J. Harris, M. Blaicher, M. K. Corrigan, T. J. Morris, W. Freude, A. Quirrenbach, and C. Koos, "Printed freeform lens arrays on multi-core fibers for highly efficient coupling in astrophotonic systems," *Opt. Express* **25**, 18288–18295 (2017).
36. A. Toulouse, S. Thiele, H. Giessen, and A. M. Herkommer, "Alignment-free integration of apertures and nontransparent hulls into 3D-printed micro-optics," *Opt. Lett.* **43**, 5283–5286 (2018).
37. S. Thiele, K. Arzenbacher, T. Gissibl, H. Giessen, and A. M. Herkommer, "3D-printed eagle eye: compound microlens system for foveated imaging," *Sci. Adv.* **3**, e1602655 (2017).
38. S. Thiele, C. Pruss, A. M. Herkommer, and H. Giessen, "3D printed stacked diffractive microlenses," *Opt. Express* **27**, 35621–35630 (2019).
39. L. Jonušauskas, D. Gailevičius, S. Rekštytė, T. Baldacchini, S. Juodkzasis, and M. Malinauskas, "Mesoscale laser 3D printing," *Opt. Express* **27**, 15205–15221 (2019).
40. Z.-C. Ma, X.-Y. Hu, Y.-L. Zhang, X.-Q. Liu, Z.-S. Hou, L.-G. Niu, L. Zhu, B. Han, Q.-D. Chen, and H.-B. Sun, "Smart compound eyes enable tunable imaging," *Adv. Funct. Mater.* **29**, 1903340 (2019).
41. J.-G. Hua, H. Ren, A. Jia, Z.-N. Tian, L. Wang, S. Juodkzasis, Q.-D. Chen, and H.-B. Sun, "Convex silica microlens arrays via femtosecond laser writing," *Opt. Lett.* **45**, 636–639 (2020).
42. T. Gissibl, S. Thiele, A. Herkommer, and H. Giessen, "Two-photon direct laser writing of ultracompact multi-lens objectives," *Nat. Photonics* **10**, 554–560 (2016).
43. T. Gissibl, M. Schmid, and H. Giessen, "Spatial beam intensity shaping using phase masks on single-mode optical fibers fabricated by femtosecond direct laser writing," *Optica* **3**, 448–451 (2016).
44. T. Gissibl, S. Thiele, A. Herkommer, and H. Giessen, "Sub-micrometre accurate free-form optics by three-dimensional printing on single-mode fibres," *Nat. Commun.* **7**, 11763 (2016).
45. A. Žukauskas, "Improvement of the fabrication accuracy of fiber tip microoptical components via mode field expansion," *J. Laser Micro/Nanoeng.* **9**, 68–72 (2014).
46. K. Weber, F. Hütt, S. Thiele, T. Gissibl, A. Herkommer, and H. Giessen, "Single mode fiber based delivery of OAM light by 3D direct laser writing," *Opt. Express* **25**, 19672–19679 (2017).
47. A. Balčytis, D. Hakobyan, M. Gabalis, A. Žukauskas, D. Urbonas, M. Malinauskas, R. Petruškevičius, E. Brasselet, and S. Juodkzasis, "Hybrid curved nano-structured micro-optical elements," *Opt. Express* **24**, 16988–16998 (2016).
48. H. E. Williams, D. J. Freppon, S. M. Kuebler, R. C. Rumpf, and M. A. Melino, "Fabrication of three-dimensional micro-photon structures on the tip of optical fibers using SU-8," *Opt. Express* **19**, 22910–22922 (2011).
49. T. Kaempfe, E.-B. Kley, and A. Tünnermann, "Hybrid approach to the design of refractive beam shaping elements," *Proc. SPIE* **5876**, 58760J (2005).
50. M. Pasiński and B. DeMarco, "A high-accuracy algorithm for designing arbitrary holographic atom traps," *Opt. Express* **16**, 2176–2190 (2008).
51. A. Jesacher, C. Maurer, A. Schwaighofer, S. Bernet, and M. Ritsch-Marte, "Near-perfect hologram reconstruction with a spatial light modulator," *Opt. Express* **16**, 2597–2603 (2008).
52. R. W. Gerchberg and W. Saxton, "A practical algorithm for the determination of the phase from image and diffraction plane pictures," *Optik* **35**, 237 (1972).
53. F. Wyrowski and O. Bryngdahl, "Iterative Fourier-transform algorithm applied to computer holography," *J. Opt. Soc. Am. A* **5**, 1058–1065 (1988).
54. T. Hessler, M. Rossi, R. E. Kunz, and M. T. Gale, "Analysis and optimization of fabrication of continuous-relief diffractive optical elements," *Appl. Opt.* **37**, 4069–4079 (1998).
55. M. T. Gale, M. Rossi, H. Schütz, P. Ehbets, H. P. Herzig, and D. Prongué, "Continuous-relief diffractive optical elements for two-dimensional array generation," *Appl. Opt.* **32**, 2526–2533 (1993).
56. H. Wang, Y. Liu, Q. Ruan, H. Liu, R. J. H. Ng, Y. S. Tan, H. Wang, Y. Li, C.-W. Qiu, and J. K. W. Yang, "Off-axis holography with uniform illumination via 3D printed diffractive optical elements," *Adv. Opt. Mater.* **7**, 1900068 (2019).
57. M. Bawart, S. Bernet, and M. Ritsch-Marte, "Programmable freeform optical elements," *Opt. Express* **25**, 4898–4906 (2017).
58. D. Infante-Gómez and H. P. Herzig, "Design, simulation, and quality evaluation of micro-optical freeform beam shapers at different illumination conditions," *Appl. Opt.* **55**, 8340–8346 (2016).
59. O. Hernandez, M. Guillon, E. Papagiakoumou, and V. Emiliani, "Zero-order suppression for two-photon holographic excitation," *Opt. Lett.* **39**, 5953–5956 (2014).
60. M. Guillon, B. C. Forget, A. J. Foust, V. De Sars, M. Ritsch-Marte, and V. Emiliani, "Vortex-free phase profiles for uniform patterning with computer-generated holography," *Opt. Express* **25**, 12640–12652 (2017).
61. H. Aagedal, M. Schmid, T. Beth, S. Teiwes, and F. Wyrowski, "Theory of speckles in diffractive optics and its application to beam shaping," *J. Mod. Opt.* **43**, 1409–1421 (1996).
62. Z. Feng, B. D. Froese, and R. Liang, "Composite method for precise freeform optical beam shaping," *Appl. Opt.* **54**, 9364–9369 (2015).
63. E.-B. Kley, M. Cumme, L.-C. Wittig, and A. Tünnermann, "Fabrication and properties of refractive micro-optical profiles for lenses, lens arrays and beam shaping elements," *Proc. SPIE* **4231**, 144 (2000).
64. L.-C. Wittig, *Kontinuierliche oberflächenprofile zur optischen strahlformung*, Ph.D. thesis (Friedrich-Schiller Universität Jena, 2005).
65. S. Schmidt, T. Tiess, S. Schröter, R. Hambach, M. Jäger, H. Bartelt, A. Tünnermann, and H. Gross, "Wave-optical modeling beyond the thin-element-approximation," *Opt. Express* **24**, 30188–30200 (2016).
66. K.-H. Brenner and W. Singer, "Light propagation through microlenses: a new simulation method," *Appl. Opt.* **32**, 4984–4988 (1993).
67. S. Schmidt, S. Thiele, A. Herkommer, A. Tünnermann, and H. Gross, "Rotationally symmetric formulation of the wave propagation method-application to the straylight analysis of diffractive lenses," *Opt. Lett.* **42**, 1612–1615 (2017).
68. S. Schmidt, T. Tiess, S. Schröter, A. Schwuchow, M. Jäger, H. Bartelt, A. Tünnermann, and H. Gross, "Noninvasive characterization of optical fibers," *Opt. Lett.* **42**, 4946–4949 (2017).
69. J.-C. Yoo and T. H. Han, "Fast normalized cross-correlation," *Circuits Syst. Signal Process.* **28**, 819–843 (2009).
70. M. Horodyski, M. Kühmayer, A. Brandstötter, K. Pichler, Y. V. Fyodorov, U. Kuhl, and S. Rotter, "Optimal wave fields for micromanipulation in complex scattering environments," *Nat. Photonics* **14**, 149–153 (2019).